TU Delft

Delft University of Technology

EM Heating-Stimulated Water Flooding for Medium–Heavy Oil Recovery

Paz, Pavel Z.S.; Hollmann, Thomas H.; Kermen, Efe; Chapiro, Grigori; Slob, Evert; Zitha, Pacelli L.J.

DOI
10.1007/s11242-017-0873-5

Publication date
2017

Document Version
Accepted author manuscript

Published in
Transport in Porous Media

Citation (APA)
Paz, P. Z. S., Hollmann, T. H., Kermen, E., Chapiro, G., Slob, E., & Zitha, P. L. J. (2017). EM Heating-Stimulated Water Flooding for Medium–Heavy Oil Recovery. *Transport in Porous Media*, *119*(1), 57 - 75. https://doi.org/10.1007/s11242-017-0873-5

Important note
To cite this publication, please use the final published version (if applicable).
Please check the document version above.

Copyright
Other than for strictly personal use, it is not permitted to download, forward or distribute the text or part of it, without the consent of the author(s) and/or copyright holder(s), unless the work is under an open content license such as Creative Commons.

Takedown policy
Please contact us and provide details if you believe this document breaches copyrights.
We will remove access to the work immediately and investigate your claim.

This work is downloaded from Delft University of Technology.
For technical reasons the number of authors shown on this cover page is limited to a maximum of 10.

© 2017 Manuscript version made available under CC-BY-NC-ND 4.0 license
https://creativecommons.org/licenses/by-nc-nd/4.0/
Postprint of Transport in Porous Media
First Online: 01 June 2017
Link to formal publication (Springer): https://dx.doi.org/10.1007/s11242-017-0873-5

Transport in Porous Media manuscript No.
(will be inserted by the editor)

EM heating stimulated water flooding for medium-heavy oil recovery

Pavel Z. S. Paz · Thomas H. Hollmann · Efe Kermen · Grigori Chapiro · Evert Slob · Pacelli L. J. Zitha

Received: date / Accepted: date

Abstract We report a study of heavy oil recovery by combined water flooding and electromagnetic (EM) heating at a frequency of 2.45 GHz used in domestic microwave ovens. A mathematical model describing this process was developed. Model equations were solved and the solution is presented in an integral form for the one dimensional case. Experiments consisting of water injection into Bentheimer sandstone cores, either fully water-saturated or containing a model heavy oil, were also conducted, with and without EM heating.

Model prediction was found to be in rather good agreement with an experiments. EM energy was efficiently absorbed by water and, under dynamic conditions, was transported deep into the porous medium. The amount of EM energy absorbed increases with water saturation. Oil recovery by water flooding combined with EM heating was up to 37.0% larger than for cold water flooding. These observations indicate that EM heating induces an overall improvement of the mobility ratio between the displacing water and the displaced heavy oil.

Keywords EOR · Electromagnetic heating · Water flooding · Partial differential equations

G. Chapiro was supported in part by Conselho Nacional de Desenvolvimento Cientfico e Tecnolgico (CNPq) under grant 470635/2012-6 and FAPEMIG under grant APQ 01377/15.

P. Paz and G. Chapiro (corresponding author)
Dep. of Mathematics, UFJF, Juiz de Fora, Brazil
Tel.: +55-32-21023308
Fax: +55-32-21023315
E-mail: grigori@ice.ufjf.br

T. H. Hollmann, E. Kermen, E. Slob and P. L. J. Zitha
Dep. of Geoscience & Engineering, TU Delft, Delft, The Netherlands

1 Introduction

Heavy and extra-heavy oil represent a large fraction of world hydrocarbon reserves. They are difficult to produce economically and the corresponding recovery factors for combined primary and secondary recovery methods hardly exceed 20-25% (Alboudwarej et al., 2006). Thermal enhanced oil recovery (EOR) methods, including hot water flooding, cyclic steam soaking, steam flooding, steam-assisted gravity drainage, in-situ combustion can increase substantially the recovery of heavy and extra-heavy oils, see (Lake, 1989; Alboudwarej et al., 2006; Farouq Ali, 1982).

EM energy conversion provides heat to porous medium much more efficiently that steam injection (Lake, 1989). For instance, in deep or low permeability reservoirs high injection pressures are needed, which leads to premature steam condensation. In highly heterogeneous formations, hot-water or steam flow preferentially through high permeability streaks, causing an uneven temperature distribution. Hot-water or steam injection are often prohibitively expensive for offshore fields due to the infrastructure required and in view of limited space available on platforms.

Downhole heating or steam generation methods, by EM induction, electric resistance heating and MW heating, emerged as a possible option to expand the envelope of hot-water and steam injection methods. They can address the above issues and can prevent environmental problems such as the melting permafrost (Alomair et al., 2012; Sahni et al., 2000; Son Tran, 2009). Low frequency resistive heating was found to be a highly efficient method to stimulate oil production, e.g., (Son Tran, 2009). However, this method may also suffer from several drawbacks, such as overheating of the electrodes located near the injection and production wells.

EM heating was introduced in 1970's (Abernethy, 1976) but did not attract much attention until recently, despite several successful field trials, (Sayakhov et al., 1970; Kasevich et al., 1994). EM heating combined with water flooding was studied numerically using a commercial simulator STARS (CMG) (Mata and Mata, 2001). However, to the best of our knowledge, there have been no attempts to treat analytically water flooding combined with EM heating and experimental data are scarce in the literature.

The purpose of this study is develop an analytical model for water-flooding combined with MW EM heating and to provide a quantitative experimental validation. We are particularly concerned with how the question of whether 2.45 GHz microwaves, similar to the domestic use, can stimulate heavy or ultra-heavy oil recovery.

Other works also propose analytical and semi-analytical methods to study nonisothermal two phase flow in porous media. For instance, no isothermal flow in the presence of tracers was studied analytically using method of characteristics (Dindoruk and Dindoruk, 2008). The model did not take into account thermal exchange with the exterior, thermal source terms and thermal diffusion along the porous media. Nonisothermal two phase flow considering thermal exchange with the exterior was studied using semi-analytical method based on

the method of characteristics for nonhomogeneous equations (LaForce et al., 2014a; Whitham, 2011). The model did not take into account thermal source terms and thermal diffusion along the porous media. The last calculations were extended to pressure and stress equations (LaForce et al., 2014b). The model addressed here takes heat diffusion into account together with heat source terms. As the resulting equations are not hyperbolic and the method of characteristics in not applicable, Duhamel's principle is used to study the problem.

The paper is organized as follows. Section 2 provides the mathematical model, which consists of a system of partial differential equations describing energy and mass balance, Darcy law and non-compressibility equation. Using the Duhamel's Principle together with the Theory of Conservation Laws we find solution to the governing equations in an integral form. Section 3 presents the water flooding experiments with and without EM conducted to check the model predictions. Section 4 offers a general discussion centered around the comparison between model and experiments. Section 6 gives the main conclusions.

2 Model

2.1 Physical model

We consider a cylindrical porous medium having a cross sectional area A and length L saturated with oil and water, which are considered immiscible. Porosity ϕ, permeability k, conate water saturation s_{wc}, viscosity μ, liquid phase density ρ are considered constants (see Tables 1 and 2). The porous medium is initially saturated with water (S_{wi}) and, eventually, with oil (S_{oi}). Obviously, in general $S_o + S_w = 1$ holds.

The medium is now subject to EM radiation from a source located near the inlet, while fluid as either static (no flow) or under dynamic conditions (flowing). EM radiation imparts a rotational motion to the molecules of dielectric materials present in the porous medium (water, oil, etc). Due to friction, the absorbed EM energy is dissipated into heat. This dielectric heating process is dominant at high frequencies (Landau et al., 1984). Its efficiency increases with the intensity of the electrical momentum dipole of the dielectric molecules. In the present case, where EM radiation has a frequency of 2.45 GHz, the efficiency of the absorption is, by far, the highest for water. Hence we assume that the water is the only material absorbing EM radiation the heat generated in the water phase will be transferred into the oil phase through convection and thermal diffusion. Thus we consider that the MW radiation is mostly absorbed by water. For the cores used (17cm), the capillary end effect should be considered but, since the permeability of the core is large, it was assumed that they are insignificant for the purpose of this study.

2.2 Governing equations

For the one dimensional case, the incompressibility condition leads to $\partial_x u = 0$, yielding constant Darcy velocity for constant injection condition. The system of equations describing our model is composed of energy balance (1), water mass balance (2) and Darcy's law (3)

$$C_{tot}\,\partial_t T + C_{liq}\,u\,\phi\partial_x T = k_m\,\partial_{xx} T + C_{ter}\,(T - T_0) + \bar{W}, \tag{1}$$

$$\phi\,\partial_t S_w + u\,\partial_x(f_w(S_w, T)) = 0, \tag{2}$$

$$u = -k\,\mu(T)^{-1}\,\nabla P, \tag{3}$$

where u $[m/s]$ is Darcy flow velocity, T [K] is temperature, S_w $[\cdot]$ is water saturation, P $[Pa]$ is pressure, C_{ter} thermal losses coefficient, C_{tot} is system thermal capacity, C_{liq} is thermal capacity of liquid phase, k_m thermal conductivity of the system. The EM energy absorption term $\bar{W}$ $[J/s]$ is given by

$$\bar{W}(x, S_w) = k_w^{em}\,S_w\,e^{-x/\bar{x}}, \tag{4}$$

where $\bar{x}$ depends on the radiation frequency, k_w^{em} is the coefficient of EM energy absorption by water, see (Landau et al., 1984) for details. This coefficient is obtained by assuming that all the EM energy is absorbed by water saturated porous medium. Generally, the coefficients C_{tot}, C_{liq} and k_m are functions of saturations and temperature. In order to obtain the analytical solution, we consider them constants as given in Tables 1 and 2. The analysis focuses on Eqs. (1)-(2) because Eq. (3) in this case corresponds to linear pressure.

Table 1 Dimensional variables and constants

Symbol	Physical quantity	Value	Unit (SI)
L	Core length	0.17	$[m]$
A	Core section area	0.00113	$[m^2]$
$\mathbf{u}$	Darcy velocity	$4.6E-3$	$[m/s]$
C_{tot}	Total thermal capacity of the system	$2.26E+06$	[J/(Km^3)]
C_{liq}	Liquid phase thermal capacity	$1.6E+06$	[J/(Km^3)]
u	Darcy velocity	$4.6E-3$	[m/s]
k_m	Matrix thermal conductivity	1.8464	[W/(mK)]
μ_w	Water viscosity	0.001	[Pa s]
μ_o	Oil viscosity	0.015	[Pa s]
S_{wc}	Conate water saturation	0.10	$[\cdot]$
S_{or}	Residual oil saturation	0.35	$[\cdot]$
k_{rw}^o	Final point of relative permeability of water	0.25	$[\cdot]$
k_{ro}^o	Final point of relative permeability of oil	0.75	$[\cdot]$
$\bar{x}$	MW characteristic length	0.1224	[m]
k_w^{em}	MW absorption coefficient	931.4	[J/(sm^3)]

We want to solve System (1)-(2) for $x \geq 0$ domain. The initial and boundary conditions will vary accordingly to the analysed experiment.

Table 2 The core-flooding experiment parameters.

Parameter \ Experiment:	5A	5B	6	7
Porous volume PV [ml]	42.6 ± 0.5	41.0 ± 0.5	40.1 ± 0.5	43.1 ± 0.5
Porosity ϕ [·]	0.22 ± 0.03	0.21 ± 0.03	0.21 ± 0.03	0.22 ± 0.03
Permeability k [D]	2.36 ± 0.10	1.83 ± 0.08	2.04 ± 0.09	2.37 ± 0.10
Initial oil sat. S_{oi} [·]	0.98 ± 0.01	0.89 ± 0.02	0.90 ± 0.02	0.86 ± 0.02

The fractional flow function is expressed in terms of viscosities and partial permeabilities using Corey model (see (Brooks and Corey, 1964)):

$$\begin{gathered} f_w = \frac{1}{1 + \frac{\mu_w}{\mu_o}\frac{k_{ro}}{k_{rw}}}, \quad S = \frac{S_w - S_{wc}}{1 - S_{wc} - S_{or}}. \\ k_{rw} = k_{rw}^0 S^2, \quad k_{ro} = k_{ro}^0 (1 - S)^2, \end{gathered} \tag{5}$$

In order to obtain analytic solutions, the dependence of the fractional flow function on temperature is neglected. For further analysis, we introduce dimensionless variables

$$\widetilde{t} = \frac{t}{t^*}, \quad \widetilde{x} = \frac{x}{x^*}, \quad \widetilde{\Theta} = \frac{T - T_0}{\Delta T^*}, \quad t^* = \frac{\phi\, L}{u}, \quad x^* = L, \quad \Delta T^* = T_0 \tag{6}$$

and rewrite the system (1)-(2) in dimensionless form (dropping tildes)

$$\partial_t \Theta + a\, \partial_x \Theta = b\, \partial_{xx} \Theta + c\, \Theta + W(x, S_w), \tag{7}$$

$$\partial_t S_w + \partial_x f_w(S_w) = 0, \tag{8}$$

$$W = \tilde{k}_m^{em} S_w \exp(-x/d), \tag{9}$$

where $a = C_{liq}\phi^2 / C_{tot}$, $b = k_m / (LuC_{tot})$, $c = LC_{ter}\phi / (uC_{tot})$, $d = \bar{x}/x^*$ and $\tilde{k}_m^{em} = (k_m^{em} L)(uC_{tot}\Delta T^*)$.

2.3 Analysis

In this section we construct an analytical solution for System (7)-(8) combining Conservation Law Theory (Method of Characteristics) and Duhamel's principle. To this end, notice that System (7)-(8) is weakly accoladed. The second equation is solved and the result is used in the first equation.

2.3.1 Water flow equation

Eq. (8) is a classical Buckley-Leverett equation, see (Buckley and Leverett, 1942). For S_w we consider a Riemann problem initial data

$$S_w(x, 0) = \begin{cases} S_w^l & x \le 0, \\ S_w^r & x > 0. \end{cases} \tag{10}$$

Thus, the solution is a sequence of one shock wave and one rarefaction wave

$$S_w(x,t) = \begin{cases} S_w^l & x \le t\, f'(S_w^l), \\ (f')^{-1}(\frac{x}{t}) & t\, f'(S_w^l) < x < t\, f'(S_w^T), \\ S_w^T & t\, f'_w(S_w^T) < x < s\, t, \\ S_w^r & x > s\, t, \end{cases} \tag{11}$$

where the shock speed is given by the Rankine-Hugoniot relation is (Smoller, 1994)

$$s = \frac{f(S_w^T) - f(S_w^r)}{S_w^T - S_w^r}. \tag{12}$$

The value S_w^T is obtained as a tangent point to the partial flow curve. Under this condition the solution given in Eq. (11) is Oleinik entropic, see (Smoller, 1994) for details.

2.3.2 Heat transport equation

In order to solve Eq. (7) we notice that systems

$$\begin{cases} \partial_t \Theta + a\, \partial_x \Theta = b\, \partial_{xx} \Theta + c\, \Theta + W \\ \Theta(x,0) = \Theta_0(x) \\ \Theta(0,t) = \Theta_l(t) \end{cases} \tag{13}$$

and

$$\begin{cases} \partial_t w = b\, \partial_{xx} w + \Phi(x,t) \\ w(x,0) = f(x) \\ w(0,t) = g(t) \end{cases} \tag{14}$$

are equivalent through the following transformation adopted from (Bhamra, 2010; Polyanin, 2001),

$$\Theta(x,t) = \exp(\beta t + \alpha x) w(x,t), \tag{15}$$

where $\alpha = a/(2b)$, $\beta = c - a^2/4b$, $f(x) = \exp(-\alpha x)\Theta_0(x)$, $g(t) = \exp(-\beta t)\Theta_l(t)$ and $\Phi(x,t) = e^{-\beta t - \alpha x} W(x, S_w)$.

Duhamel's principle consists in constructing the solution of Eq. (14) from the solution of simpler systems

$$\begin{cases} \partial_t w = b\, \partial_{xx} w + \Phi(x,t) \\ w(x,0) = 0 \\ w(0,t) = 0 \end{cases}, \quad \begin{cases} \partial_t w = b\, \partial_{xx} w \\ w(x,0) = f(x) \\ w(0,t) = 0 \end{cases}, \quad \begin{cases} \bar{x} \partial_t w = b\, \partial_{xx} w \\ w(x,0) = 0 \\ w(0,t) = g(t) \end{cases}. \tag{16}$$

Similarly to (Polyanin, 2001), the solution of Eq. (14) for $0 \le x < \infty$ and $0 < t$ is

$$w(x,t) = \int_0^\infty f(\xi)\, G(x,\xi,t)\, dy + \int_0^t g(\tau)\, H(x, t-\tau)\, d\tau + \int_0^t \int_0^\infty \Phi(\xi,\tau)\, G(x,\xi,t-\tau)\, dy\, d\tau, \tag{17}$$

where the transform kernels are given by:

$$G(x,\xi,t) = \frac{1}{2\sqrt{\pi bt}}\left\{ \exp\left[-\frac{(x-\xi)^2}{4bt}\right] - \exp\left[-\frac{(x+\xi)^2}{4bt}\right]\right\}, \tag{18}$$

$$H(x,t) = \frac{x}{2\sqrt{\pi b}t^{3/2}} \exp\left(-\frac{x^2}{4bt}\right). \tag{19}$$

For some cases we also need to consider the Neumann left boundary condition instead of Dirichlet condition. This is equivalent to substitute the boundary condition in Eq. (13) by $\partial_x \Theta = \Theta_0(x)$. The equation equivalent to Eq. (14) also changes the boundary condition to $\partial_x w(x,0) = f(x)$ with same $f(x)$. Similarly to (Polyanin, 2001), in this case, the solution is

$$w(x,t) = \int_0^\infty f(\xi)\, G(x,\xi,t)\, dy - b\int_0^t g(\tau)\, G(x,0,t-\tau)\, d\tau + \int_0^t \int_0^\infty \Phi(\xi,\tau)\, G(x,\xi,t-\tau)\, dy\, d\tau, \tag{20}$$

where the transform kernels are given by:

$$G(x,\xi,t) = \frac{1}{2\sqrt{\pi bt}}\left\{ \exp\left[-\frac{(x-\xi)^2}{4bt}\right] + \exp\left[-\frac{(x+\xi)^2}{4bt}\right]\right\},$$

$$G(x,0,t) = \frac{1}{\sqrt{\pi bt}} \exp\left(-\frac{x^2}{4bt}\right).$$

This simplified linear model does not possesses shock wave for the heat conservation equation. However, if the heat flow is modeled using partial flow functions, the equation could possibly admit shock type solution.

2.3.3 Pressure estimate

Equating the water velocity u_w expressed using the Darcy velocity $u_w = uf_w$, where f_w is given by Eq. (5) with water velocity given by Darcy's law $u_w = \lambda_w \nabla P_w$ yields

$$uf_w = \lambda_w \nabla P, \tag{21}$$

where $\lambda_w = kk_{rw}/\mu_w(T)$ and $f_w = \lambda_w/(\lambda_w + \lambda_o)$. In order to obtain the pressure drop, we divide Eq. (21) by λ_w and integrate it from the injection $x = 0$ to the first x, where water saturation s_w reaches the conate water saturation s_{wc}.

3 Experiments

3.1 Principles and Set-up

The experimental setup used in our study is shown schematically in Fig. 1. It consists of a test section in line with high precision piston displacement pump (ISCOTM), a cylinder accumulator and a fraction collector. The test section was especially designed for this study and includes a microwave (MW) generator, wave guide and, within the wave guide, the PEEK (polyetheretherketone) core-holder. The wave guide consists of a conical section with diameters 8.0 and 7.0 cm, 20.0 cm length and a hollow cylinder. It was carefully designed to guide the radiation from the MW generator towards the cylinder containing the core, while avoiding leakages of microwaves into the laboratory environment. The waveguide was placed in an earthed Faraday cage made of an Aluminum (Holland Shielding Systems) box for additional radiation shielding, see Fig. 2. Water was injected directly into the core using the ISCOTM pump. For oil injection, water was diverted to the accumulator cylinder and used to force the oil into the core.

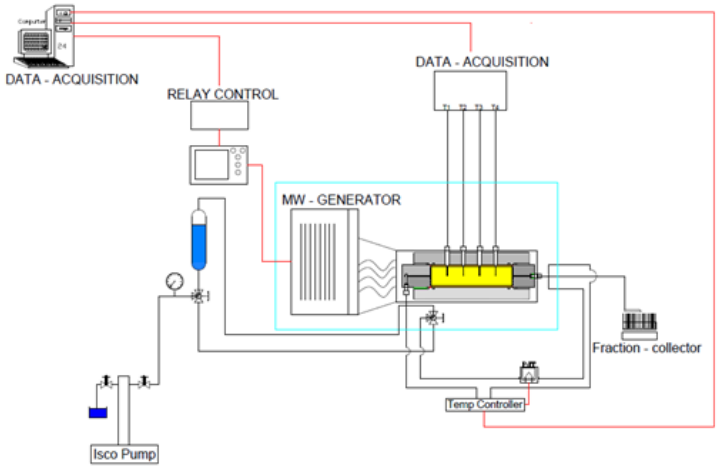

Fig. 1 Schematical representation of the setup.

Inlet and outlet temperatures were monitored using Ni-Cr/Ni-Al thermocouples with an accuracy of 0.2^oC and response time of 2.3 s. These two thermocouples were placed 5 cm from core in- and out-let. Reading of the thermocouples was done using a Tempress box temperature acquisition system.

The temperature along the core was monitored using 5 m long OpsensQR optical sensors (OTP-A) lining with PFA (perfluoroalcoxy, Teflon) and PTFE (polytetrafluoroethylene, Teflon) protective film. They were positioned at 2, 5,

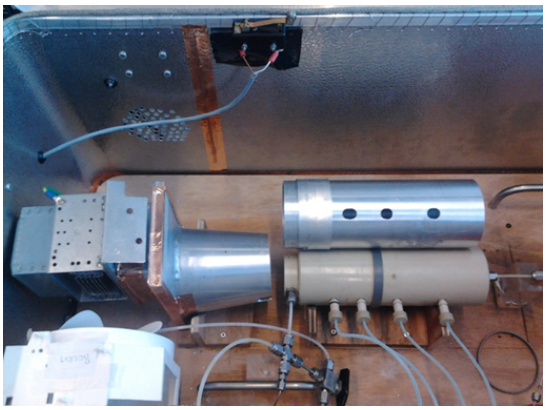

Fig. 2 The photograph shows the experimental setup inside the aluminum box.

9 and 14 cm from the injection side of the core. The sensors have an operating range of -40^oC to 250^oC and accuracy of $\pm 1^oC$. The reading of the optical sensors was done using a Multisens 4-channel signal conditioner type MUS-P4 supplied by OpsensQR. The pressure drop over the core was measured using an Endress+Hauser Deltabar transducer having a range 0-10 bar and a nominal error 0.075% of the full range (7.5 mbar). A PC and an in-house data acquisition system were used to record the pressure drop over the core and the temperatures. The PC was also used to control the switching of the MW generator.

3.2 Materials

Brine was prepared by dissolving minerals and chlorine in tap water. The main dissolved minerals are Calcium (49 mg/L) and Chloride (51 mg/L) (Lenntech Water Treatment Solutions QR). The minerals in the water are not expected to influence the experimental results, and tap water has therefore been chosen for its readily availability and low cost. The oil used in the experiments was the gear oil Omala 150 from Shell. This oil was chosen for its viscosity response to temperature changes in the interval of interest $(20 - 80^oC)$.

3.3 Porous media

Core and core-holder Bentheimer sandstone cores with a diameter 3.8 ± 0.1 cm and length 17.0 ± 0.1 cm, porosity $\phi = 21 \pm 1$ (pore volume 40.5 ± 0.1 cm^3) and permeability of approximately $k = 2$ D, were used to conduct the experiments. They were cored from a large block of about 40 cm by side. They were cut to the desired length with a water-cooled diamond saw. Thereafter cores were dried in an oven at 60^oC. Then the sandstone core was coated with a mixture

of epoxy (Huntsman CW2215) and a hardener (Huntsman REN HY5160) to prevent bypassing flow along their sides. Computer tomography (CT) images have shown that the glue penetrates $1-2$ mm into the sample, see (Simjoo et al., 2013). This reduces the cross-sectional area available for flow and should be taken into account when using the Darcy equation to calculate absolute permeability. Next, the cores were rounded at a turning lathe to precisely 4.8 ± 0.1 cm outside diameter. The optical temperature sensors penetrate 1.7 ± 0.1 cm into the core at 2.0, 5.0, 9.0 and 14.0 ± 0.1 cm from the core inlet to monitor temperature distributions. The optical sensors are led through connectors where pressure is confined by o-rings around the sensors, see Fig. 3. The connectors are screwed into the core holder, compressing the o-rings at the tip of the connector to prevent leakage along the sensors. Exact design burst pressure is unknown, but it is estimated at 40 bar, sufficient for the maximum pressure of 6.0 bar during the experiments conducted in this study. Swagelok stainless steel connectors were built in the caps to allow for flow in and out of the core holder. The annular space between the core and core holder was sealed with o-rings.

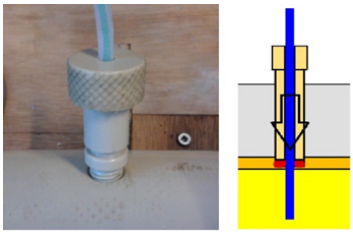

Fig. 3 The figure shows the connector through which the optical sensor enters the core-holder.

3.4 MW heating

The MW generator was recycled from a domestic microwave oven. It had an in-built relay, which controlled power supply to the transformer. The standard power settings of the microwave generator did not have enough resolution to control the temperatures within the core sufficiently. In particular the standard setting of the MW generator lead to a pulsating temperature. Therefore, in order to improve the control of the temperature a second relay was installed relay between the transformer and the MW generator. This enabled us to control more accurately the output power of the microwave and to have a uniform heating profile. By turning the microwave at full power (900 W), ensuring a constant electrical current from the transformer, and controlling the relay between the transformer and the MW generator we could control

better the power cycles. Table 3 shows the radiation output for the various power settings.

Table 3 Power cycles Samsung 900W Microwave

	100 W	300 W	450 W
Radiating time	1	7	18
Non-radiating time	30	24	10

After initial trials it was found that the MW generator was unstable and had a variable and temperature dependent start-up time. A 15 s cycle proved to be the best compromise between heating stability and a smooth heating profile (less pulsations). From basic electromagnetism it is known that radiation can propagate through holes larger than 1/4 of the wavelength, see (Landau et al., 1984). As already mentioned, the microwave antenna used in this experiment operates at a frequency of 2.45 GHz corresponding to the wavelength of about 12.2 cm. Waves should therefore have been able to exit a gap larger than 3.05 cm in diameter, a number which the exit of the conical waveguide (minimum diameter of 7.0 cm) exceeded. To ensure that the aluminum cage met the requirements of a Faraday cage the possible sources of leakage of the EM radiation were identified and the requirement measures to avoid them were taken. A microwave leakage detector was used to measure the escaping radiation along the lid and other potential leakage points of the Faraday cage. The EM radiation leaking from the waveguide and the cylindrical holder (which effectively constitute a Faraday cage themselves) was around 0.030 W/m^2. This value is much lower than the human safety threshold of 1 W/m^2.

3.5 Experiment procedure

The experimental procedure consists of the following steps. (1) The core was saturated with water under quasi vacuum conditions (0.1 bar) to ensure maximum saturation. (2) The core is weighed to quantify the pore volume. (3) The oil is placed with in the core holder and flooded with oil. When the maximum pressure drop is reached it is assumed that the connate water saturation is reached. (4) The core is then weighed again, and using the density difference between the oil and water phase the oil saturation is determined. (5) The core is flooded with water at a rate of 1.0 ml/min whilst monitoring temperature and pressure. In case of non-isothermal experiments the MW generator is used to supply heat during this phase. (6) After the experiment the water is evaporated from the test tubes in an oven, and oil rates are measured.

4 Experimental results

Eight experiments were performed. In the first three experiments, done without flow, we used the power of $P = 300$ W, see Tab. 3. We measure the heat absorption for the core saturated with water $S_w = 1$ (Experiment 1), core with maximum saturation of oil $S_w = 1 - S_{or}$ (Experiment 2) and empty core at conate water saturation $S_w = S_{wc}$ (Experiment 3). The Experiment 4 measures heat transport by cold water through the core, which was pre-heated with $P = 300$ W. Experiments 5A and 5B measured oil displacement by water injection in the absence of EM heating. Finally, experiments 6 and 7 observed enhancement of water flooding by EM radiation at $P = 114$ W and $P = 150$ W respectively.

In the present work we are mainly interested in temperature profiles used to validate the analytical solution presented in Section 2.3.

4.1 Heating without flow (Experiments 1-3)

In these experiments the temperature increase as a result of the MW absorption as plotted on the left in Fig. 4. Since the duration of the experiment was short and there was no flow, the dependence of temperature T on time t can be estimated by

$$T(t) = T_0 + \frac{P_W}{\phi C_{tot}} t, \tag{22}$$

where T_0 is the initial temperature and ϕ is porosity. From this expression the locally absorbed power P_W can be obtained as shown on the right in Fig. 4. Notice that the core saturated with water has bigger absorption than the same one with lower water content. Plotting the absorbed power profiles in a semi-log scale we obtain a strictly linear dependence. This indicates that the absorbed power is an exponentially decaying function of the distance from core inlet, motivating the model described in Section 2.

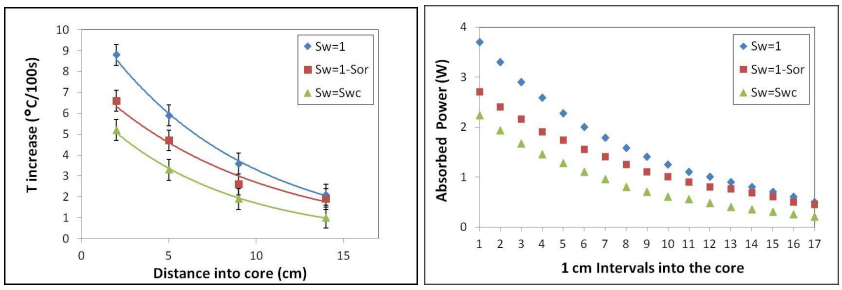

Fig. 4 The exponential trend of the temperature profiles obtained after 100 seconds of heating at 300W is shown on the left. The power absorption is plotted on the right. Three oil saturations correspond to experiments 1 ($S_w = 1$), 2 ($S_w = 1 - s_{or}$) and 3 ($S_w = s_{wc}$).

4.2 Flow without heating (Experiment 4)

A core-flood experiment was done to isolate the effect of convection on heat transport along the flow direction. First, the core was subjected to EM radiation, which increased its temperature. Then the output power was set to zero to isolate the heat transport process. Water was injected at a high flow rate (20 mL/min) to ensure that convection was dominant over diffusion. Figure 5 shows the temperature profiles obtained after switching off the microwave (Initial) at 0.5 PV intervals. The data show a heat wave moving in the flow direction, which reaches the outlet after approximately $1.5 - 2.0$ PV. During water injection the temperature at the core outlet increases from 25^oC to 45^oC. If heat losses are ignored, 74% of the initially generated heat has been transported out of the core after 2.5 PV.

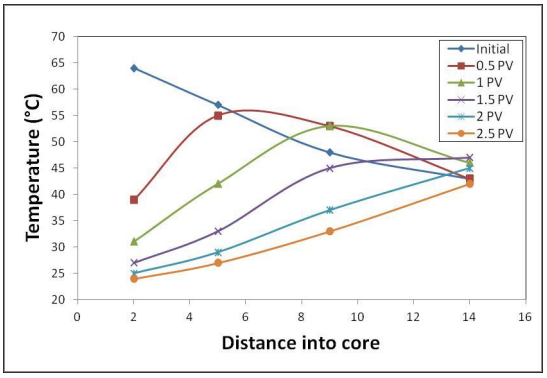

Fig. 5 Temperature profiles in the Experiment 4 at different stages of water injection. A temperature peak moves in the flow direction reaching the outlet at 2.0 PV.

4.3 Water flooding without heating (Experiments 5a and 5b)

Two baseline water flooding experiments were performed in absence of heating (microwave switched off). The experiments were done twice at exactly the same conditions to check their reproducibility. Figure 6 shows the water and oil production rates obtained in the two core-floods, corresponding to the water flooding without heating experiments 5A and 5B. These production rates were used to compute the recovery factors. It was not possible to accurately determine water breakthrough from production data because the large size of the fractions of effluents collected. However, we could obtain them from pressure drops as explained below. The recovery factors after 6 PV are respectively 0.38 ± 0.01 and 0.41 ± 0.01. These values are similar to those found in literature with the same core material but with less viscous oils, see e.g., (Simjoo et al., 2013).

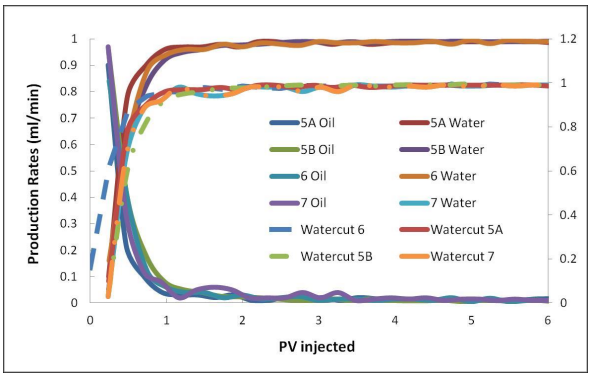

Fig. 6 The oil and water rates for the Experiments 5A, 5B, 6 and 7 together with the water-cut.

Figure 7 shows the pressure drop obtained during experiments 5A and 5B. The maximum in differential pressure is slightly lower in experiment 5B. The reason for this may be the slightly higher average temperature in the duplicate experiment ($20.4^oC \pm 1.0$ vs $21.0^oC \pm 1.0$). Due to this temperature difference the viscosities in experiments 5A and 5B may vary from 533 cP to 405 cP respectively, which means that the oil mobility of experiment 5B may be 25% higher (not taking the relative permeability change into account). From the Darcy equation we can estimate that the maximum pressure drop would be 25% lower. It can therefore be concluded that the difference in pressure drop falls well within this range, and therefore we cannot determine whether the lower maximum pressure drop was caused by the slight temperature variation. The two experiments are in good agreement, which shows that the experiments are reproducible and the newly developed set-up is adequate for studying EM heating enhanced recovery from core-floods.

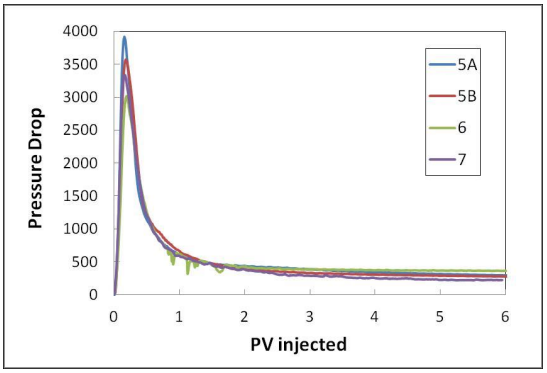

Fig. 7 The pressure drop profiles (millibar) of the Experiments 5A, 5B, 6 and 7.

4.4 Water flooding and 114 W heating (Experiment 6)

During this experiment the microwave was turned on at full power with 15 second cycles, see Tab. 3. The relay was set to allow passage of current during 28% of the pulse, or 4.2 seconds. Taking into account the pre-heating time of 2.3 seconds, the microwave emitted radiation for the remaining 1.9 seconds. This corresponds to 114 W of output power averaged over a 15 second cycle.

From the analysis of the initial temperature increase (heat losses are at a minimum due to low differential temperatures) it is deduced that on average over the total length of the core 12 Watt is converted to heat by the connate water. At residual oil saturation this is increased to around 27 Watts. As explained earlier there are large uncertainties associated with this number due to (1) the variation of necessary pre-heating time, (2) instability of the MW generator and (3) the adjustments made to the power supply during the experiments to prevent over- and under-heating. Figure 8 shows the temperatures in the core during Experiment 6. The average temperature in the core during the experiment was 33.8^oC. The large variations of the temperature profiles are a result of modulations of the microwave output power. From 0 to about 1 PV the temperatures increase sharply, and after approximately 0.8 PV leakages occurred, therefore the output power of the microwave was lowered.

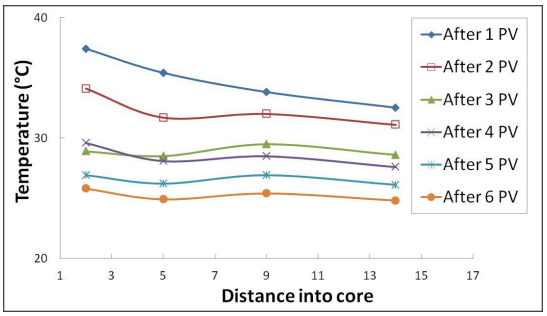

Fig. 8 Temperature distributions at 1 PV injected intervals during Experiment 6.

The profiles show that the highest temperatures were reached after 1 PV injected, and that temperatures rose fastest near the sensor closest to the microwave antenna. In later stages the temperature at the inlet is lower than further into the core due to arrival of colder injected water. Overall the profiles show a cooling trend resulting from lowering lowering the MW output power to prevent leakage. The slightly higher temperatures registered at the third sensor (9 cm) fall within the measurement error of the optical sensors (1^oC) and should therefore be ignored.

As can be seen in Fig 6, from 0 to 1.5 PV the oil rates are lower than for the water flooding without heating (5A and 5B). However, from 1.5 to 6 PV oil rates are slightly higher, which indicates an increase recovery factor (dura-

tion of the experiments is nearly the same). This is confirmed by the recovery factors plotted in Figure 10, together with those of the other experiments. The recovery factor for the experiment 6 after 6 PV was 0.44 ± 0.02. This represents an increase of 11% on average compared to the water flooding without heating cases (5A and 5B). The question arises now of whether the incremental recovery will also increase if we increase the power of the EM radiation. To answer this question an experiment was performed at a higher MW power.

The pressure drop obtained during water flooding and 114 W heating is shown in Fig. 7. The maximum pressure drop is slightly lower (less than 20%) than in the experiments without heating. Furthermore, there are some fluctuations around the main trend of the pressure drop profile. These variations are a consequence of leakage problems, explained above. The leakage problem was solved during the experiment, and total fluid losses were less than 1.0 mL. Therefore the experiment was still considered valuable. When compared to the isothermal cases, water breakthrough is on average delayed by 19%. A temperature increase would lower the oil/water mobility ratio, leading to a higher shock front saturation and a delay in water breakthrough. However, at the water breakthrough time, temperatures have not yet risen significantly and the delay of breakthrough might be caused by heterogeneities in the sandstone.

4.5 Water flooding and 114 W heating (Experiment 7)

During the experiment the relay was set to allow passage of the current during 34% of the 15 second cycle, or 4.8 seconds. Taking into account the startup time, the microwave is expected to deliver 150 W of output power for the duration of the experiment. From the initial temperature increase it is deduced that on average over the total length of the core 15 W is converted to heat by the water at connate water saturation. At residual oil saturation this is increased to about 35 W.

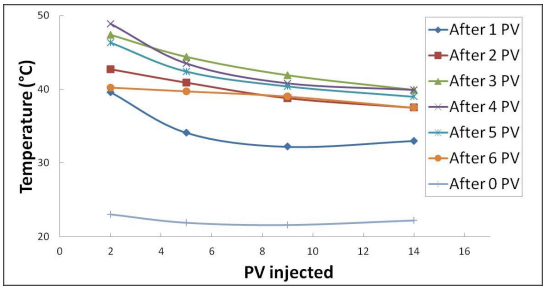

Fig. 9 Temperature distributions at 1 PV injected intervals during the Experiment 7.

Fig. 9, on the left hand side, shows that the temperature has an overall increasing trend, with fairly large fluctuations. The oscillations are due to ad-

justments in heating power. Fig. 9, on the right hand side, shows that the temperature decreases slightly from the inlet to the outlet of the core as result of higher power absorption at the inlet. The oil production rate in this experiment is slightly lower than the one at 114 W heating (Exp. 6) up to approximately 1 PV. After 1 PV the oil production rate is slightly higher, a result of the higher temperatures reached in the later stages of the experiment. The recovery factor after 6 PV injected water was 0.54 ± 0.02 is shown in Fig. 10. It is 37% higher than in the case of water flooding without heating (5A and 5B). This confirms that the oil recovery factor can be increased by increasing the power of the EM radiation.

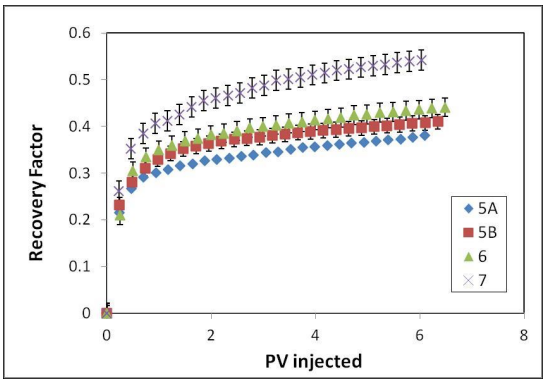

Fig. 10 Oil production for the Experiments 5A, 5B, 6 and 7.

The pressure drop throughout this experiment was plotted in Fig. 7. Compared to the isothermal cases 5A and 5B, water breakthrough is not significantly delayed. The pressure drop at breakthrough is 12% lower than the isothermal experiments. It falls within the error range and is therefore insignificant.

5 Comparison of model and experiments

The procedure consists in numerical integration of Eq. (17) (or Eq. (20)) using the exact solution for S_w given by Eq. (11). Next we use Eq. (15) to obtain the temperature profile.

We compare the analytical solution with the experimental results in three cases: heating under no flow conditions, with $S_w = 1$ (Experiment 1), heat transport inside the pre-heated core (Experiment 4), water flooding and MW heating (Experiment 7).

Experiment 1 In this case (no flow) water saturation is constant and the System (1)-(2) reduces to the first equation only. Initial data for T is a constant

ambient temperature. For the left Dirichlet boundary condition the solution given by Eq. (17) is plotted in Fig. 11 at different times. For long distances (typically > 0.08 m) the model predictions (solid lines) is in excellent agreement with the experimental data (dots and dashed lines). For short distances the agreement between the model and experiments is not as good. We believe that this is due to fluctuations in the temperature inherent to experiments. The dimensionless parameters in this case are $a = 0$; $b = 8.09712e-07$; $c = 4.88281e-05$.

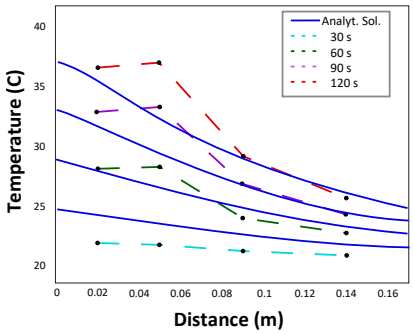

Fig. 11 Temperature profile using analytical solution describing no flow Experiment 1.

We note a more systematic and larger difference between model and experiments for the shortest time (30 s). This could be due to thermal losses. These are expected to be significant initially but they will diminish over time as the air in the aluminum box is heated up.

Experiment 4 In this case water was injected at ambient temperature into a preheated core saturated with brine (see Fig. 5). In absence of MW heating, the source term W is zero. The initial condition for T used to derive the analytical solution is the one obtained from the experiments at the end of the preheating period. For the left Neumann boundary condition the solution is given by Eq. (20). The solution for the case without thermal losses ($C_{ter} = 0$) is plotted on the left side in Fig. 12. The case with thermal losses, estimated using least square method, is plotted on the right side in Fig. 12. The obtained thermal losses coefficient is $C_{ter} = -1.75E-04$ (corresponding to dimensionless parameters $a = 2.08729e-04$; $b = 8.09712e-07$; $c = -1.5e-4$). The experimental data are shown by dots and dashed lines for different times. The model predictions (solid lines) is in good agreement with the experimental data.

For the same reasons detailed in the previous paragraphs the quality of the match between the model and the experiments for long times is not so good as for short ones.

Experiment 7 In this case we injected water at ambient temperature into the core. The MW heating was set at an average power $P = 150$ [W] as explained

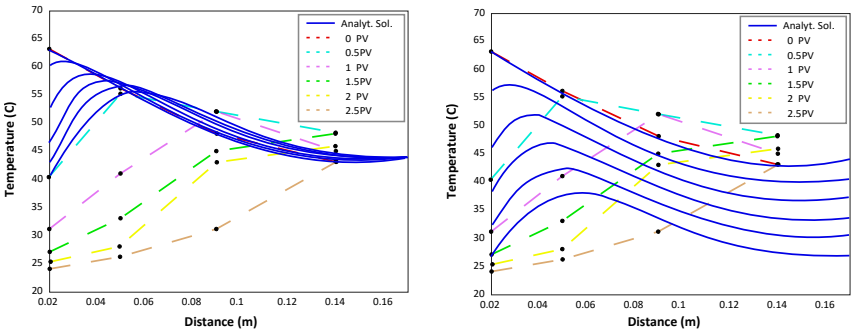

Fig. 12 Temperature profile using analytical solution describing Experiment 4 with no thermal losses ($C_{ter} = 0$) on the left side and using $C_{ter} = -1.75E-04$ on the right side.

in Section 4. Similarly to the previous cases the initial condition for T used to derive the analytical solution was the one obtained from the experiments at starting time. Dirichlet boundary condition was used leading to the analytical solution expressed by Eq. (20). The solution for the case with no thermal losses ($C_{ter} = 0$) is plotted on the left side in Fig. 13. The experimental data are shown by dots and dashed lines for different times. In this case no match could be obtained between the model predictions (solid lines) and experiments. In fact, the experiments exhibit an upward concave shape wile the model present a downward concave shape. This suggests that leaving out the thermal losses does not represent correctly the physics of the problem. To address this issue we estimated thermal losses coefficient by least square method. The result is plotted on the right side in Fig. 13 and the corresponding coefficient is $C_{ter} = -3.75e-05$ (corresponding to dimensionless parameters $a = 5.21822e-05$; $b = 8.09712e-07$; $c = -3.90625e-4$). In this figure can be seen than the model predictions and experiments are good qualitative agreement. This underscores significance of thermal losses in the investigated case. We note further that the analytical solution reaches an equilibrium after approximately 2 PV. The oil and water viscosities decrease according to an Arrhenius law.

Notice that the effect of the increasing power of the EM source at the inlet, according to our analysis, does not modify the solution but clearly the conversion of energy leads to higher temperature.

Pressure A quantitative match between the measured and calculated pressures is unlikely to obtained for two main reasons: Firstly the model ignores the dependence of the fluid mobilities when solving the equations for the saturations. Secondly the parameters used in the calculations are obtained from the literature which could be rather different than those actually corresponding to the studied rock fluid system. Nevertheless some useful considerations can be made from a qualitative comparison.

The pressure drop was estimated directly using the water saturation profile as explained in Sec. 2.3.3. In order to capture the qualitative behavior

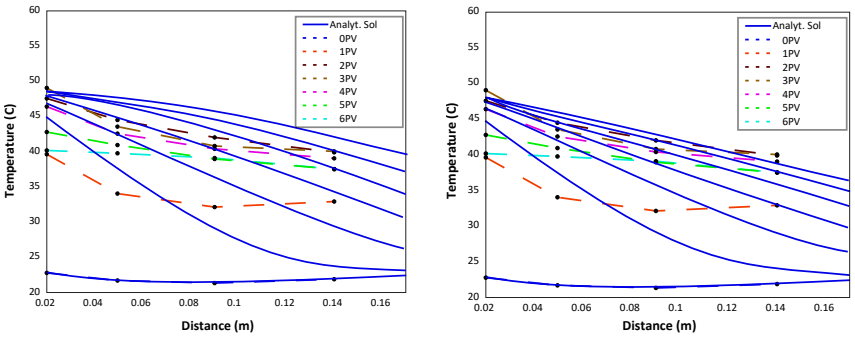

Fig. 13 Temperature profile using analytical solution describing Experiment 7 with no thermal losses ($C_{ter} = 0$) on the left side and using $C_{ter} = -3.75e - 05$ on the right side.

observed in the measured pressure drops plotted in Fig. 7, some parameters were modified ($k^o_{rw} = 0.1$, $k^o_{ro} = 0.9$ and $\mu_o = 0.06$). The resulting simulation is plotted in Fig. 14. Notice that the measured and calculated pressure drops are equal at long times, which indicates an acceptable fit.

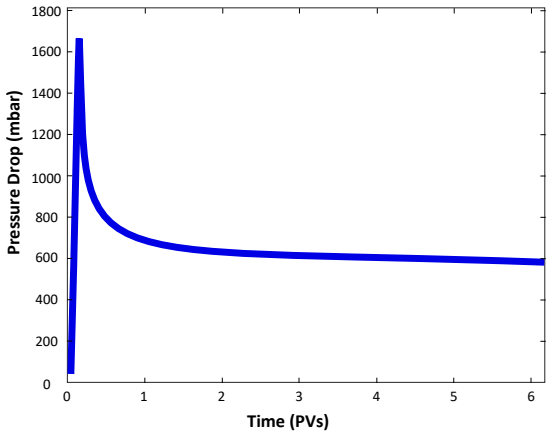

Fig. 14 Pressure drop (millibar) estimated using water saturation as explained in Sec. 2.3.3.

6 Conclusions

A model describing EM stimulated water flooding was developed and then solved analytically resulting in an integral form for the temperature. The latter was solved numerically for several practically relevant cases. EM stimulated water flooding experiments were also conducted using a suitably modified core-

flooding set-up fitted with a 2.45 GHz microwave source. In this study we found that:

1. Sandstone cores saturated with water and oil were successfully heated using EM radiation and temperature decays exponentially as function of distance from the EM source.
2. Power absorption increased with water saturation and the pre-generated heat at no-flow conditions was transported effectively by the subsequent flow of water.
3. Up to water breakthrough time, EM heating resulted only in a small change of the two phase-flow pattern due to the limited amount of heat generated (breakthrough was only slightly delayed). At later times, higher temperatures were achieved resulting in an substantial increase of the total oil production, 37.0% at 6.0 PV.
4. Unfortunately, in this study the experiments were done without CT scanning. For this reason comparison such measured saturation profiles and calculated ones was not possible. Future works should address this issue.

From both modeling and experiments it can be concluded that EM stimulated water flooding is potentially highly effective method for enhancing medium and heavy oil recovery.

Acknowledgements We gratefully acknowledge Hans Bruining for the thorough reading of an earlier version of the manuscript and his many useful suggestions. We would also like to thank Paul Vermeulen, Marc Friebel, Dick Delforterie and Karl Heller for their technical support. We thank Dirk van der Lei from Holland Shielding Systems b.v. for his guidance in making the set-up as safe as possible. We thank Stiw Harrison Herrera Taipe, Iuri Higor Aguiar da Igreja and anonymous referee for help in improving this text.

References

H. Alboudwarej, J. Felix, S. Taylor, R. Badry, C. Bremner, B. Brough, C. Skeates, A. Baker, D. Palmer, and K. Pattison. Highlighting heavy oil. *Oilfield review*, 18(2):34–53, 2006.

L. W. Lake. *Enhanced oil recovery*. Old Tappan, NJ; Prentice Hall Inc., 1989.

S.M. Farouq Ali. Steam injection theories: a unified approach. Technical report, 1982.

O. A. Alomair, M. A. Alarouj, A. A. Althenayyan, A. H. Al Saleh, H. Almohammad, Y. Altahoo, Y. Alhaidar, S. E. Al Ansari, and Y. Alshammari. Improving heavy oil recovery by unconventional thermal methods. In *SPE Kuwait International Petroleum Conference and Exhibition*. SPE, 2012.

A. Sahni, M. Kumar, and R. B. Knapp. Electromagnetic heating methods for heavy oil reservoirs. In *SPE/AAPG Western Regional Meeting*. SPE, 2000.

T. Son Tran. Electromagnetic assisted carbonated water flooding in heavy oil recovery. Master's thesis, TU Delft, 2009.

E. R. Abernethy. Production increase of heavy oils by electromagnetic heating. *Journal of Canadian Petroleum Technology*, 15(03), 1976.

F.L. Sayakhov, G.A. Babalyan, and S.I. Chistyakov. On the high-frequency heating bottomhole zone. *Neft. Khoz*, 12:49–66, 1970.

R.S. Kasevich, S.L. Price, D.L. Faust, and M.F. Fontaine. Pilot testing of a radio frequency heating system for enhanced oil recovery from diatomaceous earth. In *SPE Annual Technical Conference and Exhibition*. SPE, 1994.

W Mata and A.L. Mata. Electromagnetic heating process combined with water displacement for recovering petroleum reservoirs-a new concept. In *Canadian International Petroleum Conference*. Pet. Society of Canada, 2001.

D.M. Dindoruk and B. Dindoruk. Analytical solution of nonisothermal buckley-leverett flow including tracers. *SPE Reservoir Evaluation & Engineering*, 11(03):555–564, 2008.

T LaForce, J Ennis-King, and L Paterson. Semi-analytical solutions for non-isothermal fluid injection including heat loss from the reservoir: Part 1. saturation and temperature. *Advances in Water Resources*, 73:227–241, 2014a.

G. B. Whitham. *Linear and nonlinear waves*, volume 42. John Wiley & Sons, 2011.

T LaForce, A Mijić, J Ennis-King, and L Paterson. Semi-analytical solutions for nonisothermal fluid injection including heat loss from the reservoir: Part 2. pressure and stress. *Advances in Water Resources*, 73:242–253, 2014b.

L. D. Landau, E. M. Lifshitz, and L. P. Pitaevskii. *Electrodynamics of continuous media*, volume 8. Pergamon, 2 edition, 1984.

R.H. Brooks and T. Corey. Hydraulic properties of porous media. *Hydrology papers of Colorado State University*, 1964.

S. E. Buckley and M.C. Leverett. Mechanism of fluid displacement in sands. *Transactions of the AIME*, 146(01):107–116, 1942.

J. Smoller. *Shock Waves and Reaction-Diffusion Equations*. Springer-Verlag, New York, NY, 2^{nd} edition, 1994.

K.S. Bhamra. *Partial differential equations*. PHI Learning Pvt. Ltd., 2010.

A. D. Polyanin. *Handbook of linear partial differential equations for engineers and scientists*. CRC press, 2001.

M. Simjoo, Y. Dong, A. Andrianov, M. Talanana, and P.L.J. Zitha. Novel insight into foam mobility control. *SPE Journal*, 18(03):416–427, 2013.